THE JOURNAL OF BIOLOGICAL CHEMISTRY VOL. 286, NO. 35, pp. 30732–30739, September 2, 2011

Molecular Basis of Actin Nucleation Factor Cooperativity

CRYSTAL STRUCTURE OF THE SPIR-1 KINASE NON-CATALYTIC C-LOBE DOMAIN (KIND)·FORMIN-2 FORMIN SPIR INTERACTION MOTIF (FSI) COMPLEX[*][S]

Received for publication, May 4, 2011, and in revised form, June 10, 2011 Published, JBC Papers in Press, June 26, 2011, DOI 10.1074/jbc.M111.257782

Kornelius Zeth[‡1], **Markos Pechlivanis**[§1], **Annette Samol**[§], **Sandra Pleiser**[§], **Clemens Vonrhein**[¶], **and Eugen Kerkhoff**[§2]

From the [‡]*Department of Protein Evolution, Max Planck Institute for Developmental Biology, Spemannstrasse 35, 72076 Tübingen, Germany, the* [§]*Department of Neurology, Molecular Cell Biology Laboratory, Bavarian Genome Research Network (BayGene), University Hospital Regensburg, Franz-Josef-Strauss-Allee 11, 93053 Regensburg, Germany, and* [¶]*Global Phasing Limited, Sheraton House, Castle Park, Cambridge CB3 0AX, United Kingdom*

The distinct actin nucleation factors of the Spir and formin subgroup families cooperate in actin nucleation. The Spir/formin cooperativity has been identified to direct two essential steps in mammalian oocyte maturation, the asymmetric spindle positioning and polar body extrusion during meiosis. Understanding the nature and regulation of the Spir/Fmn cooperation is an important requirement to comprehend mammalian reproduction. Recently we dissected the structural elements of the Spir and Fmn family proteins, which physically link the two actin nucleation factors. The trans-regulatory interaction is mediated by the Spir kinase non-catalytic C-lobe domain (KIND) and the C-terminal formin Spir interaction motif (FSI). The interaction inhibits formin nucleation activity and enhances the Spir activity. To get insights into the molecular mechanism of the Spir/Fmn interaction, we determined the crystal structure of the KIND domain alone and in complex with the C-terminal Fmn-2 FSI peptide. Together they confirm the proposed structural homology of the KIND domain to the protein kinase fold and reveal the basis of the Spir/formin interaction. The complex structure showed a large interface with conserved and positively charged residues of the Fmn FSI peptide mediating major contacts to an acidic groove on the surface of KIND. Protein interaction studies verified the electrostatic nature of the interaction. The data presented here provide the molecular basis of the Spir/formin interaction and give a first structural view into the mechanisms of actin nucleation factor cooperativity.

The dynamic arrangement and rearrangement of the actin cytoskeleton are mandatory for cells to fulfill an impressive spectrum of tasks such as cell migration, vesicular transport processes, reorganization of cellular substructures, or the regulation of morphological dynamics. The amazing diversity of these cellular actin functions is reflected in a rapidly increasing number of regulatory mechanisms directing the dynamic assembly and disassembly of actin filaments (1). A specific prerequisite to set up the distinct actin structures is the spatial and temporal regulation of filament initiation. Due to the relative instability of the actin dimer and monomeric G-actin-binding proteins, the initiation of actin polymerization from free monomers (nucleation) requires factors that help to overcome the kinetic barrier to nucleation (1).

Three different classes of actin nucleation factors have been described so far that function in the nucleation of actin filaments, firstly the actin-related protein 2/3 (Arp2/3) complex, secondly nucleation factors of the formin superfamily, and thirdly nucleation factors containing from one to multiple WH2 domains (2). Spir proteins are the founding members of the latter class of actin nucleation factors, the Wiskott-Aldrich syndrome protein homology 2 (WH2) domain-containing nucleators (3, 4). Spir nucleation activity resides in a cluster of four actin-binding WH2 domains in the central region of the protein (3). Although Spir proteins are capable of nucleating actin polymerization *in vitro* by themselves, they were also found to act in cooperation with the distinct actin nucleators of the formin subgroup (Fmn)[3] of formins (*Drosophila melanogaster* Cappuccino protein and its two vertebrate homologs formin-1 (Fmn-1) and formin-2 (Fmn-2)) (5, 6). The *Drosophila spire* and *cappuccino* mutants were indentified in the same genetic screen and have an identical phenotype (7, 8). Later it was shown that both proteins regulate a common actin meshwork in the *Drosophila* oocyte that suppresses premature cytoplasmic streaming (9). Very recently mouse Spir-1 and Spir-2 were described to cooperate with the mouse Cappuccino homolog formin-2 protein in regulating a similar actin meshwork in mouse oocytes, which is required for asymmetric spindle positioning during meiosis (10). The proteins in addition colocalized at the cleavage furrow during polar body extrusion, which was found to be dependent on Spir function. Spir/formin cooperation is therefore considered to be a major regulatory function in mammalian oocyte maturation and is thought to be an essential mechanism in human reproduction.

* This work was supported by the Bavarian Genome Research Network (BayGene) and the German Research Foundation (DFG SPP 1135, SPP 1464) (to E. K.) and DFG SPP 1464 and the Max Planck Society (to K. Z.).

The atomic coordinates and structure factors (codes 2YLF and 2YLE) have been deposited in the Protein Data Bank, Research Collaboratory for Structural Bioinformatics, Rutgers University, New Brunswick, NJ (http://www.rcsb.org/).

[S] The on-line version of this article (available at http://www.jbc.org) contains supplemental Figs. S1 and S2 and Tables S1–S4.

[1] Both authors contributed equally to this work.

[2] To whom correspondence should be addressed. Tel.: 49-941-944-8920; Fax: 49-941-944-8921; E-mail: eugen.kerkhoff@klinik.uni-regensburg.de.

[3] The abbreviations used are: Fmn, formin subgroup of formins; KIND, kinase non-catalytic C-lobe domain; FSI, formin Spir interaction motif; eGFP, enhanced green fluorescent protein; PAK, p21-activated kinase; TAO2, thousand-and-one amino acid kinase 2; Ni-NTA, nickel-nitrilotriacetic acid; r.m.s., root mean square.

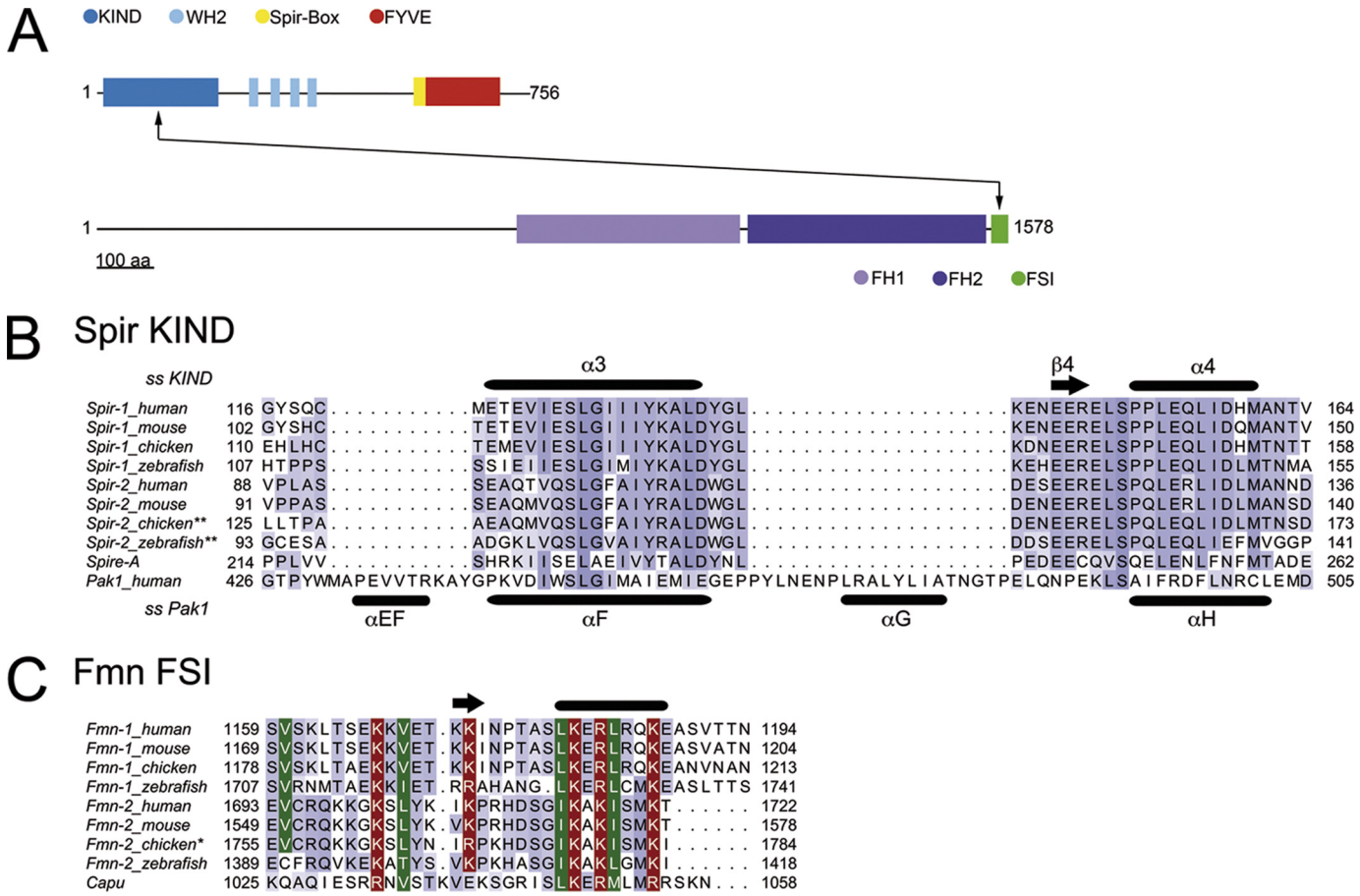

FIGURE 1. **Domain organization of Spir and Fmn family proteins.** *A*, the domain organization of the human Spir-1 and the mouse Fmn-2 proteins is shown. The regulatory interaction of the Spir-1-KIND domain and the Fmn-2-FSI domain is indicated by *arrows*. *B* and *C*, multiple sequence alignments of the interaction regions of Spir KIND in comparison with PAK1 kinase (Pak1_human) (*B*) and Fmn FSI sequences (*C*). The sequences were aligned by a ClustalW multiple sequence alignment and manually realigned when necessary. *Arrows* and *tubes* above the sequence alignment mark regions with β-sheet and α-helical structure, respectively. Protein accession numbers are listed in supplemental Table S1. * indicates a discrepancy between the genomic sequence and the expressed sequence tag clone that was used for the alignment. ** indicates that no full-length sequences of Spir for these species were available. Color coding is as follows: conserved residues are in *blue shadings* (Blosum 62 score; conservation threshold: 0.1), highly conserved basic residues within the FSI are shown in *red*, and highly conserved aliphatic residues are shown in *green*, respectively. *Capu*, cappuccino.

In line with the genetic and cellular studies, biochemical studies uncovered a direct physical interaction of Spire and Cappuccino, as well as a direct interaction of the mammalian homologs, Spir-1, -2, and formin-1, -2 (5, 6, 11). It was shown that the N-terminal Spir KIND domain interacts with the C-terminal part of the formin protein comprising the FH2 domain and flanking regions. By *in vitro* actin polymerization studies, it could be shown that the interaction of the KIND domain with a C-terminal construct of formin enhances the nucleation activity of Spir and blocks the nucleation activity of the formin construct (5, 11). In an ongoing study, it was found that this interaction was mediated by binding of the Spir KIND domain to a highly conserved short sequence motif C-terminal adjacent to the FH2 domains (formin Spir interaction motif, FSI) (Fig. 1, *A* and *C*) (6).

The KIND domain was discovered as a conserved N-terminal Spir region that shares sequence homology to the C-lobe of protein kinases (12). The catalytic protein kinase fold harbors two structurally independent subdomains, an N-lobe mainly formed by β-sheets that contributes to ATP binding and a predominantly α-helical C-lobe that contains the catalytic residues and the activation loop (13). In between the two lobes, the catalytic cleft is located, where the ATP is bound and the γ-phosphate is transferred to a receiving hydroxyl group of the target protein (see Fig. 3). Due to the absence of the N-lobe and the active site residues in the catalytic and activation loops, it was suggested that it folds independently and is non-catalytic (12). KIND domains have been identified in four different protein families to date: the Spir actin nucleators, the Ras guanine exchange factor very-KIND, the protein tyrosine phosphatase Basophil-like/Basophil (PTP-BL/BAS), and the multi-PDZ domain protein FRMPD2 (12, 14–16). Its late occurrence in evolution led to the speculation that the KIND domain evolved from the catalytic protein kinase into an interaction domain possibly by keeping substrate binding features.

To get further insights into the molecular mechanism of the Spir/Fmn interaction, we determined the crystal structure of the Spir-1-KIND·Fmn-2-FSI complex and have verified the crystallographic data by protein interaction studies. This study provides the first structural characterization of a KIND domain. Additionally it reveals the interaction surface of the mammalian Spir·formin actin nucleator complex, which serves as the molecular basis to understand the cooperativity of these two actin nucleation factors.

EXPERIMENTAL PROCEDURES

Expression Vector Cloning—For the expression of recombinant Spir and formin proteins in bacteria and mammalian cells, DNA expression vectors were generated by standard cloning methods. Point mutants have been generated with the QuikChange site-directed mutagenesis kit (Agilent, Stratagene). The following primers have been used (only the coding strand primers are shown, and mutations are underlined): hs-Spir-1 D138N, 5′-gga att att att tat aaa gca ctg aac tat ggt ttg aag gag aat gaa gaa-3′; hs-Spir-1 Y134K, 5′-gaa tct ttg gga att att att aag aaa gca ctg gac tat ggt ttg-3′; mm-Fmn-2 K1571A, 5′-ccg aga cat gac tct ggg att gca gcg aag ata agc atg aaa acg-3′; mm-Fmn-2 K1571E, 5′-ccg aga cat gac tct ggg att gaa gcg aag ata agc atg aaa acg-3′. Supplemental Tables S1 and S4 summarize the individual constructs and give a brief description of the National Center for Biotechnology Information (NCBI) gene/protein accession numbers, fragment boundaries, purification scheme, and their purpose in the study (supplemental Tables S1 and S4).

Protein Expression and Purification—Recombinant Spir and formin proteins were expressed and purified as described before (6). Briefly *Escherichia coli Rosetta* pLysS bacteria were transformed with plasmid DNA expression vectors encoding for glutathione *S*-transferase (GST) and His_6-tagged recombinant Spir and formin proteins, respectively. Bacteria were lysed by ultrasonication, and soluble proteins were purified by incubation with glutathione (GSH)-Sepharose (GE Healthcare) or nickel-nitrilotriacetic acid (Ni-NTA) agarose (Qiagen) affinity beads. Alternatively the proteins were purified with an ÄKTA purifier system (GE Healthcare) using Ni-NTA affinity (Ni-NTA HP), GSH affinity (GSH-Sepharose FF) and size exclusion (Sephadex G200) chromatography according to the manufacturer's recommendations. His_6 and GST tags were cleaved where indicated by tobacco etch virus protease (supplemental Fig. S2).

Crystallization and Data Collection of the KIND Domain and the KIND·FSI Complex—Crystallization of the Spir-1-KIND domain was initiated using the wild-type protein or the selenomethionine derivative at 10 mg/ml in gel filtration buffer (20 mM Tris, pH 7.4, 100 mM NaCl, 2 mM dithioerythritol). Initial protein crystals were obtained by the sitting drop crystallization method using 1000 crystallization conditions (400 conditions for the selenomethionine derivative) on the basis of commercial screens (Hampton Research, Jena Bioscience, Qiagen). Sitting drops were prepared using the Honeybee 961/963 robot (Digilab Genomic Solutions) in 96-well plates at 18 °C mixing 400 nl of protein and reservoir solution each. Crystals of the KIND domain appeared under several conditions. Crystals taken from a drop containing 20% PEG 8000, 0.1 M Tris, pH 8, were taken and shortly incubated in a solution containing the reservoir solution supplemented with 15% PEG 400. Crystals were cryo-mounted by freezing them in liquid nitrogen. Crystals of the selenomethionine derivative were obtained under the following conditions (25% PEG 3350, 0.1 M Hepes, pH 7.5) and directly frozen in liquid nitrogen. Crystals of the KIND·FSI complex were obtained under essentially the same experimental conditions as described for the KIND domain alone. The protein in gel filtration buffer was mixed with a 2-fold excess of the peptide containing the terminal 29 residues of human formin-2 (Fig. 1*C*, *Fmn-2_human*, amino acids 1694–1722 = FSI peptide), and crystals appeared under differing conditions (20% PEG 6000, 0.1 M Tris, pH 8). These crystals (typically 50 × 50 × 200 μm in size) were mounted by a short incubation step using the reservoir solution and adding 10% PEG 400. The crystals were frozen as described for the KIND domain alone.

Data Collection and Structure Determination of KIND and KIND·FSI—All datasets were collected at the PXII beamline of the Swiss Light Source (SLS). Data of the Spir-1-KIND domain alone (to 2.65 Å resolution for crystal form I in space group $P3_221$ and 2.7 Å for crystal form II in space group P1) were collected at 90 K and λ = 1 Å. Diffraction images were recorded on an MAR225 detector system (MarResearch, Norderstedt, Germany) at exposure times of 1 s, beam attenuation to 20%, and rotation angles of 1°. For the Se-Met derivative, the wavelength was adjusted to λ = 0.978 Å, and a dataset of 360 images (1 s, 1° rotation) at a beam attenuation of 5% to 3.5 Å resolution was collected. The entire Se-Met dataset was merged and used for the initial phasing of the domain. Crystals of the KIND·FSI complex diffracting to 1.8 Å in space group $P3_221$ were collected under the same conditions as described for wild-type KIND, but data were recorded on a Pilatus 6M (Dectris) detector system. All diffraction images were processed and scaled with the XDS/XSCALE program package (17).

Heavy atoms were identified using autoSHARP, initial phases were calculated using the selenomethionine dataset and crystal averaging finally extended to the native 2.7 Å by Solomon, and automatic model building in Buccaneer allowed tracing of significant parts of the protein model (18–20). The model was manually expanded based on the single anomalous dispersion-phased density, and model refinement against data of 2.05 Å resulted in good statistics (Table 1). Model building and refinement were performed in CCP4 (21) and Coot (22). Protein geometry was analyzed using the program PROCHECK (23) and RAMPAGE server, and secondary structures were assigned based on the Dictionary of Secondary Struture of Proteins (DSSP) algorithm (24). The structure of the KIND·FSI complex was solved by molecular replacement using the KIND domain structure as the search model. The structure of the complex was rebuilt as described for KIND domain alone and refined to R/R_{free} factors of 0.18/0.23. Statistics are summarized in Table 1. Pictures were prepared using the PyMOL program package, and molecular contacts and contact interface areas were analyzed using the PISA server.

GST Pulldown Assays—GST pulldown experiments were performed as described before (6). Bacterially expressed GST or GST-Spir-1-KIND proteins were coupled to GSH-Sepharose 4B beads (GE Healthcare). The beads were incubated with total cell lysates of HEK-293 cells, which transiently expressed eGFP-tagged proteins. Bound proteins were analyzed by SDS-PAGE and subsequent Western blot analysis. For immunodetection, the following primary antibody was used: anti-GFP Living Colors A.v. peptide antibody (rabbit polyclonal, 1.0 μg/ml, Clontech). The proteins were visualized with the enhanced chemiluminescence kit from GE Healthcare. Experimental data were digitalized with an Image Quant LAS 4000 CCD camera

TABLE 1
Data collection and refinement statistics
Values in parentheses are for highest-resolution shell.

	Spir-1-KIND	Spir-1-KIND·Fmn-2-FSI
Data collection		
Space group	$P3_221$	$P3_221$
Cell dimensions		
a, *b*, *c* (Å)	65.91, 65.19, 78.80	65.67, 65.67, 77.94
α, β, γ (°)	90, 90, 120	90, 90, 120
Resolution (Å)	33-2.05 (2.17-2.05)	28.4-1.8 (1.92-1.8)
R_{sym} or R_{merge}	0.079 (0.42)	0.082 (0.74)
$I/\sigma I$	14.15 (2.81)	12.24 (2.34)
Completeness (%)	97.5 (94.2)	96.2 (95.6)
Redundancy	4.0 (3.8)	5.5 (5.6)
Refinement		
Resolution (Å)	33-2–05 (2.10-2.05)	28.4-1.8 (1.85-1.8)
No. of reflections	11,995	16,921
R_{work}/R_{free}	0.20/0.26 (0.28/0.32)	0.18/0.23 (0.23/0.27)
No. of atoms		
Protein	1309	1622
Water	106	90
B-factors		
Protein	31.3	21.7
Water	35.5	25.5
r.m.s. deviations		
Bond lengths (Å)	0.023	0.012
Bond angles (°)	1.8	1.22
Ramachandran statistics		
Favored region	153 (98.1%)	181 (98.4%)
Allowed region	3 (1.9%)	2 (1.1%)
Outlier region	0 (0.0%)	1 (0.5%)
PDB entry	2YLF	2YLE

imaging system (GE Healthcare) and a PEQLAB gel documentation system and further processed with Adobe Photoshop.

Cell Culture, Transfections, Immunostains, and Fluorescence Microscopy—Human cervical cancer cells (HeLa) and human embryonic kidney 293 cells (HEK-293) were cultured, transfected, and stained as described before (6). Briefly transient transfections with eukaryotic expression vectors were performed with the Lipofectamine reagent (Invitrogen). Cells were assayed 24–36 h after transfection. For immunostaining, the cells were fixed with 3.7% paraformaldehyde and stained by employing 5 μg/ml anti-c-Myc 9E10 mouse monoclonal antibody (Santa Cruz Biotechnology). The immunofluorescence and protein autofluorescence were analyzed with a Leica AF6000LX imaging system. Images were saved as TIFF files using the Leica Application Suite AF software and further processed with Adobe Photoshop.

RESULTS

Structural Basis of Spir·Formin Complex Formation—The structure of the KIND-only domain was determined at 2.05 Å and shows an almost complete α-helical fold (helices α1–α6) with a small three-stranded β-sheet close to the N terminus of the molecule (for further details, see Fig. 2, *A* and *C*). Both termini are closely related in space. The overall structure is flexible with two loops not visible in the electron density. Five helices (α1–α5) together form the core of the module and are structurally aligned almost parallel relative to each other. Only the longest C-terminal α6-helix is located slightly apart with an angle of ~90° relative to the helix bundle (Fig. 2*A*). The structure of the Spir-1-KIND domain in complex with the Fmn-2-FSI motif was determined at 1.8 Å resolution and is compared with the isolated KIND structure, almost identical with a small r.m.s. deviation of 0.4 Å.

Upon binding of the FSI peptide representing the terminal 29 residues of formin-2, a local restructuring is visible in KIND, and an additional β-strand (β4) becomes visibly ordered from a previous loop structure, which was not well ordered in the KIND domain (Fig. 2*A*). The interface between the FSI peptide and the KIND domain is significantly large with almost 1000 Å^2. The N-terminal part of the FSI (amino acids 1702–1711) is almost fully extended and stabilized by KIND mostly through H-bonds (*e.g.* via β-sheet pairing) and salt bridges (Fig. 3*A*; see supplemental Table S2 for specific interactions). The C-terminal part of FSI, which forms the α-helical portion of the peptide, interacts with the KIND domain basis (residues 1712–1722; Fig. 2, *B* and *C*; see also supplemental Table S2). The *B*-factors of this helix part are lower than for the N-terminal extended portion presumably through the embedding into the groove structure offered by the KIND surface (data not shown). Interestingly only 4 of the 21 residues on FSI that were visible in the crystal structure are not involved in molecular interactions (see supplemental Table S3).

A refined analysis of the interaction network between the FSI and the KIND domain reveals a large number of 13 H-bonds and six salt bridges (see the stereo figure in Fig. 3*A* and supplemental Table S2 for more details). There are a significant number of conserved residues on both the FSI and the KIND domains (Figs. 1, *B* and *C*, and 3*B*). The FSI peptide is preferentially positively charged (residues Lys-1707, Arg-1709, Lys-1715, Lys-1717, Lys-1721), with most residues conserved among the formin homologs shown in Fig. 1*C*. Residues on the KIND counter surface are predominantly negatively charged (Fig. 2*D*) and also conserved (Fig. 1*B*). Helices 3 and 4 are particularly involved in the interactions to the FSI peptide employing the negatively charged residues Asp-138, Glu-146, Glu-148, and Asp-158 of the KIND domain. All of these residues are conserved among the Spir family KIND domains, but only a small subset is also conserved as far as the homologous kinase structure is concerned (Fig. 1*B*).

The search of the KIND domain coordinates against the Protein Data Bank (PDB) using the DALI program returned a number of kinases, two of which were the PAK1 (PDB entry 1YHV, r.m.s. deviation for 136 aligned residues 2.9 Å) and the TAO2 kinases (PDB entry 1U5R, r.m.s. deviation for 145 residues 2.9 Å) (25). The archetypical characteristic of a kinase is the two-domain organization into the N-terminal and C-terminal lobe subdomains (13). Another archetypical feature of these domains is the ATP cofactor that is tightly bound between these two domains. A superposition of KIND with these kinases revealed the analogy in the C-lobe structure, whereas the N-lobe structure is missing in the Spir protein (Fig. 3*C*).

Mutational Analysis of the KIND/FSI Interaction—The structural analysis of the Spir-1-KIND·Fmn-2-FSI complex confirmed that the highly conserved basic amino acids in the C-terminal part of the formin FSI establish major electrostatic contacts with the acidic binding surface of the KIND domain (Figs. 1 and 3*A*, supplemental Table S2). We identified aspartate 138 (Asp-138) in the center of the interaction surface of the Spir-1-KIND domain forming a salt bridge and hydrogen bond to the conserved lysine Lys-1715 (in mouse, Lys-1571) within the FSI motif. To test the interaction data from the crystalliza-

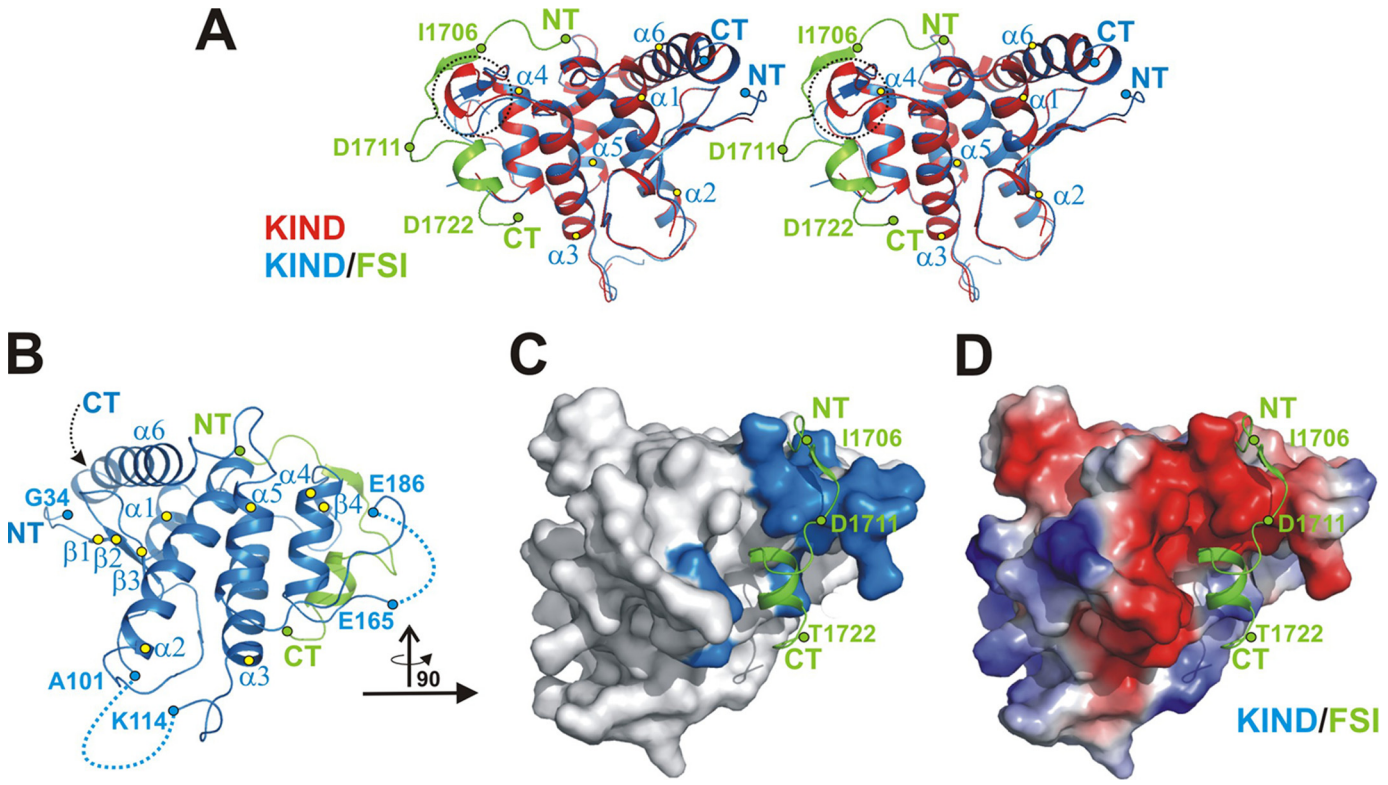

FIGURE 2. **Structure comparison of the isolated Spir-1-KIND domain and the Fmn-2-FSI·Spir-1-KIND complex.** *A*, stereo view ribbon model of the isolated KIND structure in *red* and the complex structure of KIND·FSI in *blue* (KIND) and *green* (FSI), respectively. Secondary structure elements are indicated with α1–α6 and β1–β4, and both termini are marked. The major structural change between the two KIND domains is the reorganization of the β4-sheet upon binding of the peptide (encircled with a *dashed line*). All figures were prepared using the PyMOL program package. *B*, structure representation of the KIND·FSI complex in graphic representation with the KIND domain colored in *blue* and the FSI colored in *green*, respectively. Structure elements missing in the x-ray structure due to flexibility are indicated by *dashed lines*. *Blue dots* indicate amino acids at the borders of loops that are not visible in the electron density map. All secondary structure elements are marked with α1–α6 and β1–β4 and *yellow points* for better visibility. *C*, structure of the KIND·FSI complex tilted by 90° relative to *B*. The KIND domain is shown in surface representation, and the FSI (*green*) is shown in graphic representation. Contact areas on the KIND surface are marked in *blue*. For clarity, anchor points have been added to the FSI, shown as *green dots*. *D*, same orientation of the complex as in *C* with the KIND domain surface representing the charge distribution. Positively charged areas are marked in *blue*, whereas negatively charged areas are marked in *red*.

tion studies, we have mutated Asp-138 of the KIND domain to asparagine (Spir-1-KIND-D138N) to impair the salt bridging. In GST pulldown assays employing bacterially expressed GST-Spir-1-KIND proteins coupled to glutathione-Sepharose beads and a total lysate of HEK-293 cells transiently expressing an eGFP-tagged C-terminal Fmn-2 protein, the mutated KIND domain failed to pull down the eGFP-tagged C-terminal Fmn-2 fusion protein (eGFP-Fmn-2-FH2-FSI), which, however, interacted strongly with the wild-type KIND domain in these assays (Fig. 4*A*). No interaction was detected with the GST protein alone (Fig. 4*A*).

To further verify the interaction surface, we have mutated the corresponding basic amino acid Lys-1571 within the Fmn-2-FSI motif to alanine. The eGFP-tagged Fmn-2-FH2-FSI K1571A mutant protein showed a strongly reduced to non-detectable interaction with the Spir-1-KIND domain when compared with the very strong interaction of the wild-type Fmn-2-FH2-FSI protein (Fig. 4*B*). In these assays, in addition to the KIND D138N mutant, we also included a KIND mutant in which we introduced a positive charge into the acidic groove of the KIND domain by replacement of tyrosine 134 to lysine (Y134K). The Y134K mutation reduced the binding of the eGFP-Fnm-2-FH2-FSI protein to the same extent as the D138N mutant did (Fig. 4*B*).

The eGFP-Fmn-2-FH2-FSI protein has an even cytoplasmic distribution when expressed in mammalian cells. We have shown before that targeting of the Spir-1-KIND domain to the cell membrane and intracellular membranes structures by an H-Ras-CAA*X* motif leads to a translocation and perfect colocalization of the eGFP-Fnm-2-FH2-FSI protein with the Spir-1-KIND domain (5). Here we employed the cellular protein interaction assay to analyze the Spir/formin interaction surface. Mutation of the conserved basic lysine Lys-1571 within the Fmn-2-FSI sequence into the acidic amino acid glutamate (Lys-1571) leads to a failure of the eGFP-Fmn-2-FH2-FSI K1571E protein to translocate toward the membrane-targeted Spir-1-KIND-CAA*X* protein (Fig. 4*C*). When coexpressed in HeLa cells, the mutated formin protein kept its even cytoplasmic distribution and did not colocalize with Myc-Spir-1-KIND-CAA*X* protein at the cell membrane and cytoplasmic spots (Fig. 4*C*).

DISCUSSION

The study depicted here presents the first atomic structure of a KIND domain, which confirms the proposed structural similarity of the KIND domain with the protein kinase fold and supports the function of the KIND domain as a protein interaction module. The KIND domain was discovered as a highly conserved N-terminal region on the Spir protein class that shares sequence homologies to the C-lobe of protein kinases (12). In contrast to the protein kinase fold that harbors two

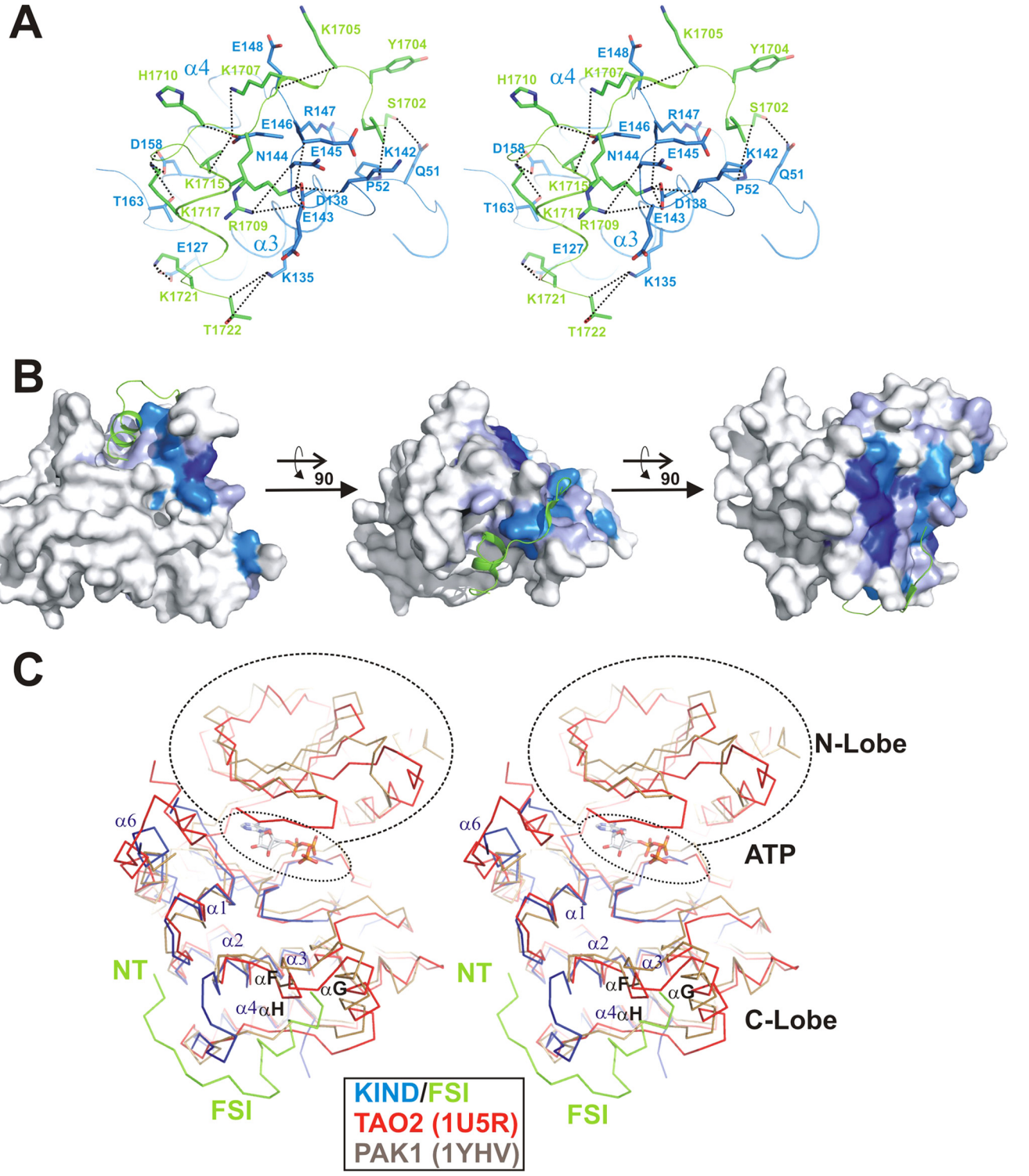

FIGURE 3. **Structure of the KIND·FSI interface and analysis of the molecular structure.** *A*, stereo view of the molecular interface of the KIND domain in *blue* and the FSI peptide in *green*. Interacting residues are marked in stick representation, and H-bonds as well as salt bridges are indicated by *dashed lines*. Additional information underlying this graphic is presented in supplemental Table S2. *B*, surface representation of KIND from three different views, connected by 90° relative to each other. Conserved residue patches are marked in *blue*, (for conservation score, see supplemental Fig. S1) whereas the FSI peptide is marked in *green*. *C*, architectural comparison of the KIND domain and closely related kinases TAO2 (PDB entry, 1U5R) and PAK1 (PDB entry, 1YHV) (25, 27). All structures are depicted in ribbon representation, the individual kinase domains are marked with N- and C-lobe, and the ATP-binding site located between the two lobe domains is *encircled*. Helices superimposed between the kinase PAK1 and the KIND domains are marked with Greek and Roman letters(*αF*, *αG*, and *αH* for PAK1 and *α3* and *α4* for KIND).

structurally independent subdomains, an N-lobe mainly formed by β-sheets and a mainly α-helical C-lobe, the fold of the KIND domain mimics only the C-lobe of the kinase fold. The absence of the structural equivalent to the kinase N-lobe results in the lack of ATP binding, and the mutation of important catalytic active site residues in the catalytic and activation

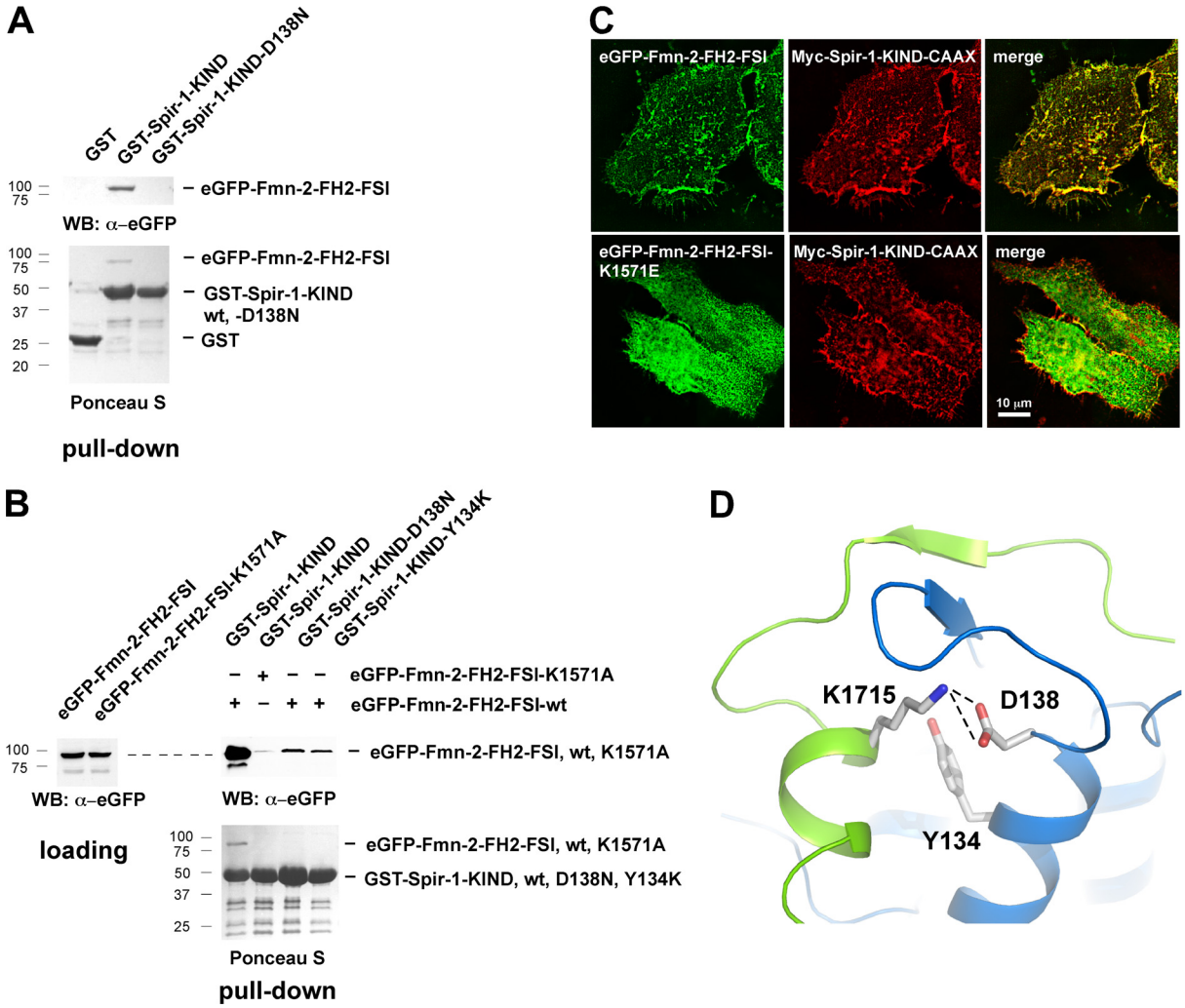

FIGURE 4. **Mutational analysis of the Spir-1-KIND/Fmn-2-FSI interaction.** *A* and *B*, the interaction of the Spir-1-KIND domain with C-terminal Fmn-2 constructs has been analyzed by GST pulldown experiments. For mutational analysis, the Spir-1-KIND D138N and Y134K and the Fmn-2-FH2-FSI K1571A mutants have been employed. Ponceau S staining of the bacterially expressed purified GST and GST-Spir-1-KIND (D138N, Y134K) and immunoblots (*WB*) of pulled and loaded eGFP-Fmn-2-FH2-FSI (K1571A) proteins from HEK-293 lysates are shown. The employed antibody is indicated (*WB: α-eGFP*). *C*, the translocation of the eGFP-Fmn-2-FH2-FSI proteins toward a membrane-targeted Myc-Spir-1-KIND-CA*AX* protein is dependent on the conserved Fmn-2 basic residue Lys-1751. The protein localization of two coexpression experiments in HeLa cells transiently expressing eGFP-Fmn-2-FH2-FSI or eGFP-Fmn-2-FH2-FSI K1571E and Myc-Spir-1-KIND-CA*AX* was detected by immunofluorescence (Myc tag) and autofluorescence (eGFP tag). Deconvoluted (blind) fluorescence microscopy pictures of single and merged channels are shown. *D*, the positions of the residues targeted in the mutational analysis (*A–C*) are highlighted in the Spir-1-KIND (*blue*)·Fmn-2-FSI (*green*) complex structure (human Spir-1 Asp-138, human Spir-1 Tyr-134, and human Fmn-2 Lys-1715, which corresponds to mouse Fmn-2 Lys-1571). A complex structure section of the interaction surface is shown.

loops suggests that the KIND domain is non-catalytic (12). The KIND crystal structure presented here clearly confirms this proposed structural similarity. The alignment with the TAO2 and PAK1 kinases shows that the tertiary structure of the KIND domain almost perfectly overlaps with the three-dimensional array of the kinase C-lobe (Fig. 3*C*).

However, when comparing the crystal structures of a similar protein kinase·substrate complex, *i.e.* the PKA·PKI complex and the PAK kinase with its inhibitory switch region (PDB entries: 1ATP/1F3M) (26, 27), with the KIND·FSI complex, the proposed protein-binding sites are significantly different between the classical kinases and the KIND domain (Fig. 5). Protein kinase A (PKA, PDB entry 1ATP) binds the PKI inhibitor peptide, which is structurally similar to the FSI, at a different location when compared with the KIND·FSI complex, and the same is true for the inhibitory switch region of PAK (26, 27). Up until now, one could not exclude that additional substrates of the KIND domain bind to sites that are more equivalent to the substrate-binding sites of common kinases.

Two KIND domain-interacting proteins have been identified (5, 6, 28, 29). The formin subgroup actin nucleators interact with the Spir KIND domain, and the microtubule-associated protein 2 (MAP2) interacts with the second KIND domain of the RasGEF very-KIND. In preliminary studies, we recently identified a protein involved in the regulation of microtubule dynamics as an interaction partner of the protein tyrosine phosphatase Basophil-like/Basophil (PTP-BL/BAS) KIND domain,[4] pointing toward a general function of KIND domains as protein interaction modules in the cytoskeletal organization.

[4] A. Pawelec and E. Kerkhoff, unpublished observations.

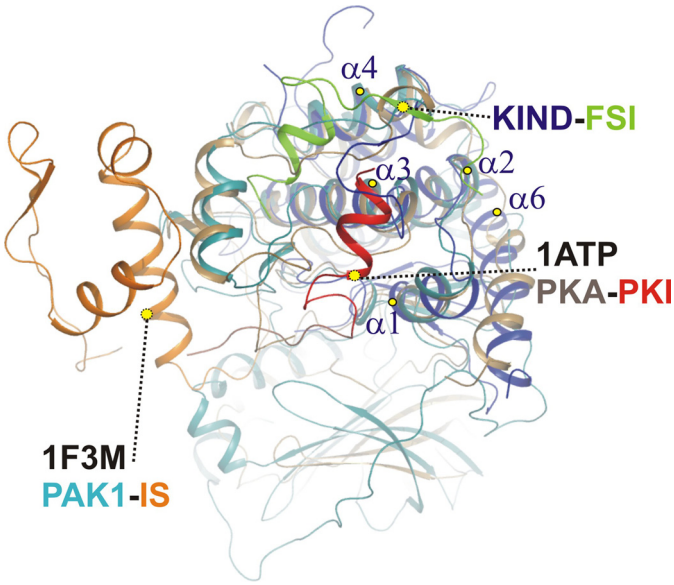

FIGURE 5. **Superposition of the Spir-1-KIND·Fmn-2-FSI, PAK1 (PDB entry, 1F3M) (27), and PKA·PKI (PDB entry, 1ATP) (26) structures.** The interacting peptides of the KIND domain and the kinase complexes are marked in *orange* (PAK kinase inhibitory switch region (*PAK1-IS*)), *red* (PKI), and *green* (Fmn-2-FSI) and indicate the distant localization relative to the KIND·kinase C-lobe core domains.

As a mechanism of highest interest, the distinct actin nucleation factors of the Spir and formin subgroup proteins cooperate in actin organization (9, 10). The proteins form a complex and control the generation of cytoplasmic actin meshworks in *Drosophila* and mammalian oocytes in a cooperative way. The findings that the formin proteins in this complex might function as nucleation-promoting factors and actin polymerization factors rather than as nucleators has opened a new view on the role of formins in the regulation of the actin cytoskeleton (30), and only recently, a similar mechanism was proposed for the novel actin nucleator adenomatous polyposis coli (APC) and the formin mDia (31). The KIND·FSI structure shown here provides the first structural insights into the cooperative Spir formin nucleation mechanism. The basic residues within the Fmn-2-FSI motif target an acidic groove on the surface of the KIND domain, which is part of an extended area of a highly conserved residual patch on the surface of the KIND domain (Fig. 3). The large interface between KIND and FSI components also underlines our previous *in vitro* data of a strong interaction in the nanomolar range (6). The FSI β1 structural element is the C-terminal extension of the formin FH2 domain, which forms a ring-structured dimer and binds actin proteins for the initiation of actin polymerization (32). The formin nucleation activity is blocked by the interaction with the KIND domain (5). It is tempting to speculate that the FH2 sequences contact the conserved extension on the KIND surface, and by this method, arrange the KIND domain in a way so that it blocks actin assembly for nucleation. This is supported by experiments showing that an extended FSI peptide (eFSI), which encodes additional C-terminal FH2 domain sequences, has a slightly higher KIND domain affinity than the FSI sequence motif alone (6).

Based on the cell biological function of the Spir·Fmn complex in mammalian oocyte maturation, understanding the nature and regulation of the Spir/Fmn cooperation is a necessary requirement to comprehend human/mammalian reproduction. Additional structural studies comprising multiple domains of the nucleation factors or even the full-length proteins will be necessary to fully understand the cooperative mechanism in the future.

Acknowledgments—We thank Michael Eck and Margot Quinlan for discussion. The help of Reinhard Albrecht in the sample preparation and crystallization process and the support of people from the PXII beamline at SLS are highly appreciated.

REFERENCES

1. Pollard, T. D., and Cooper, J. A. (2009) *Science* **326,** 1208–1212
2. Qualmann, B., and Kessels, M. M. (2009) *Trends Cell Biol.* **19,** 276–285
3. Quinlan, M. E., Heuser, J. E., Kerkhoff, E., and Mullins, R. D. (2005) *Nature* **433,** 382–388
4. Dominguez, R. (2010) *Curr. Opin. Struct. Biol.* **20,** 217–225
5. Quinlan, M. E., Hilgert, S., Bedrossian, A., Mullins, R. D., and Kerkhoff, E. (2007) *J. Cell Biol.* **179,** 117–128
6. Pechlivanis, M., Samol, A., and Kerkhoff, E. (2009) *J. Biol. Chem.* **284,** 25324–25333
7. Manseau, L. J., and Schüpbach, T. (1989) *Genes Dev.* **3,** 1437–1452
8. Wellington, A., Emmons, S., James, B., Calley, J., Grover, M., Tolias, P., and Manseau, L. (1999) *Development* **126,** 5267–5274
9. Dahlgaard, K., Raposo, A. A., Niccoli, T., and St Johnston, D. (2007) *Dev. Cell* **13,** 539–553
10. Pfender, S., Kuznetsov, V., Pleiser, S., Kerkhoff, E., and Schuh, M. (2011) *Curr. Biol.* **21,** 955–960
11. Rosales-Nieves, A. E., Johndrow, J. E., Keller, L. C., Magie, C. R., Pinto-Santini, D. M., and Parkhurst, S. M. (2006) *Nat. Cell Biol.* **8,** 367–376
12. Ciccarelli, F. D., Bork, P., and Kerkhoff, E. (2003) *Trends Biochem. Sci.* **28,** 349–352
13. Knighton, D. R., Zheng, J. H., Ten Eyck, L. F., Ashford, V. A., Xuong, N. H., Taylor, S. S., and Sowadski, J. M. (1991) *Science* **253,** 407–414
14. Erdmann, K. S. (2003) *Eur. J. Biochem.* **270,** 4789–4798
15. Mees, A., Rock, R., Ciccarelli, F. D., Leberfinger, C. B., Borawski, J. M., Bork, P., Wiese, S., Gessler, M., and Kerkhoff, E. (2005) *Gene Expr. Patterns* **6,** 79–85
16. Stenzel, N., Fetzer, C. P., Heumann, R., and Erdmann, K. S. (2009) *J. Cell Sci.* **122,** 3374–3384
17. Kabsch, W. (1993) *J. Appl. Crystallogr.* **26,** 795–800
18. Keegan, R. M., Long, F., Fazio, V. J., Winn, M. D., Murshudov, G. N., and Vagin, A. A. (2011) *Acta Crystallogr. D Biol. Crystallogr.* **67,** 313–323
19. Vonrhein, C., Blanc, E., Roversi, P., and Bricogne, G. (2007) *Methods Mol. Biol.* **364,** 215–230
20. Abrahams, J. P., and Leslie, A. G. (1996) *Acta Crystallogr. D Biol. Crystallogr.* **52,** 30–42
21. Murshudov, G. N., Vagin, A. A., and Dodson, E. J. (1997) *Acta Crystallogr. D Biol. Crystallogr.* **53,** 240–255
22. Emsley, P., and Cowtan, K. (2004) *Acta Crystallogr. D Biol. Crystallogr.* **60,** 2126–2132
23. Laskowski, R. A., MacArthur, M. W., Moss, D. S., and Thornton, J. M. (1993) *J. App. Crystallogr.* **26,** 283–291
24. Kabsch, W., and Sander, C. (1983) *Biopolymers* **22,** 2577–2637
25. Zhou, T., Raman, M., Gao, Y., Earnest, S., Chen, Z., Machius, M., Cobb, M. H., and Goldsmith, E. J. (2004) *Structure* **12,** 1891–1900
26. Zheng, J., Knighton, D. R., ten Eyck, L. F., Karlsson, R., Xuong, N., Taylor, S. S., and Sowadski, J. M. (1993) *Biochemistry* **32,** 2154–2161
27. Lei, M., Lu, W., Meng, W., Parrini, M. C., Eck, M. J., Mayer, B. J., and Harrison, S. C. (2000) *Cell* **102,** 387–397
28. Huang, J., Furuya, A., and Furuichi, T. (2007) *J. Cell Biol.* **179,** 539–552
29. Huang, J., Furuya, A., Hayashi, K., and Furuichi, T. (2011) *FEBS J.* **278,** 1651–1661
30. Quinlan, M. E., and Kerkhoff, E. (2008) *Nat. Cell Biol.* **10,** 13–15
31. Okada, K., Bartolini, F., Deaconescu, A. M., Moseley, J. B., Dogic, Z., Grigorieff, N., Gundersen, G. G., and Goode, B. L. (2010) *J. Cell Biol.* **189,** 1087–1096
32. Otomo, T., Tomchick, D. R., Otomo, C., Panchal, S. C., Machius, M., and Rosen, M. K. (2005) *Nature* **433,** 488–494